Revista de la Academia Colombiana de Ciencias Exactas, Físicas y Naturales.
47(185):795-806, octubre-diciembre de 2023. doi: https://doi.org/10.18257/raccefyn.1952

Physical Sciences

Original article

Geometric uncertainty in non-paraxial interference

Incertidumbre geométrica en interferencia no-paraxial

Román Castañeda

Escuela de Física, Facultad de Ciencias, Universidad Nacional de Colombia Sede Medellín, Colombia

Abstract

In this article, a novel meaning for the notion of uncertainty is discussed, within the framework of the non-paraxial interference theory based on confinement in geometric states of space. This novel meaning refers to the fact that, for any set of space states whose vertices are distributed in an arbitrary array of size less than $\lambda/10$, both the excitation provided by the geometric potential and the positions of the vertices of the states are completely uncertain, such that the complete set is represented by the Lorentzian well of an individual ground state of space, with vertex at any of the points of the array, even if the set is under the maximum prepared non-locality (i.e., under a strong geometric potential). It is shown that the geometric uncertainty is different but compatible with the Heisenberg uncertainty principle. In fact, geometrical uncertainty establishes both the upper limit of momentum uncertainty and the lower limit of position uncertainty in the Heisenberg principle.

Keywords: Uncertainty; States of space; Geometric potential; Confinement; Spatially structured wells.

Resumen

En este artículo se discute un significado novedoso para la noción de incertidumbre, en el marco de la teoría de interferencia no-paraxial basada en el confinamiento en estados geométricos del espacio. Este significado se refiere al hecho de que, para cualquier conjunto de estados del espacio cuyos vértices se distribuyen en un arreglo arbitrario de tamaño menor que $\lambda/10$, tanto la excitación proporcionada por el potencial geométrico como las posiciones de los vértices de los estados son completamente inciertas, de tal forma que el conjunto completo es representado por el pozo lorentziano de un estado base individual del espacio, con vértice en cualquiera de los puntos del arreglo, incluso si el conjunto está bajo la máxima no-localidad preparada (es decir, bajo potencial geométrico fuerte). Se muestra que la incertidumbre geométrica es diferente pero compatible con el principio de incertidumbre de Heisenberg. De hecho, la incertidumbre geométrica establece tanto el límite superior de la incertidumbre de cantidad de movimiento como el límite inferior de la incertidumbre de posición en el principio de Heisenberg.

Palabras clave: Indeterminación; Estados del espacio; Potencial geométrico; Confinamiento; Pozos espacialmente estructurados.

Introduction

Uncertainty is a principle of quantum mechanics that precludes the simultaneous measurement of conjugated variables, such as position and momentum or time and energy, with arbitrary accuracy (**Feynman *et al,*** 1965). Because such simultaneous measurement is required for describing particle dynamics deterministically, uncertainty limits the deterministic knowledge of physical systems.

Preclusion of simultaneous accurate measurement of conjugated variables (u,v) is usually formalized by the canonical inequality $\Delta u\,\Delta v \geq \alpha\hbar$, with $\Delta u, \Delta v$ denoting the uncertainties of the measured variables, α is a real positive number (usually 1/2) and $\hbar = h/2\pi$ with h the Planck's constant (**Feynman *et al*,** 1965). Thus, if measurement accuracy of any of them, say u, arbitrarily increases so that $\Delta u \to 0$, then the uncertainty of the other variable increases arbitrarily, i.e. $\Delta v \to \infty$, thus impeding its accurate measurement.

Citation: Román C. Geometric uncertainty in non-paraxial interference. Revista de la Academia Colombiana de Ciencias Exactas, Físicas y Naturales. 47(185):795-806, octubre-diciembre de 2023. doi: https://doi.org/10.18257/raccefyn.1952

Editor: Angela Guzmán

***Corresponding autor:**
Román Castañeda;
rcastane@unal.edu.co

Received: July 17, 2023
Accepted: November 26, 2023
Published on line: December 7, 2023

Revista de la Academia Colombiana de Ciencias Exactas, Físicas y Naturales.
47(185):795-806, octubre-diciembre de 2023. doi: https://doi.org/10.18257/raccefyn.1952

Single particle diffraction by slit masks has been used for demonstrating uncertainty between position and momentum, i.e. Heisenberg's uncertainty principle (**Feynman *et al*,** 1965*;* **Matteucci *et al*,** 2010). Slit width is associated to the uncertainty of the transverse position component Δx of the particle that crosses the slit, while main maximum width of far-field diffraction pattern is associated to the uncertainty of the transverse component of particle momentum Δp. So, paraxially approached diffraction (**Born & Wolf,** 1993) allows verifying the achievement of Heisenberg's uncertainty principle $\Delta x\,\Delta p \geq \hbar/2$ straightforwardly.

Although this description of uncertainty is widely accepted, some authors have indicated important precisions that not only improve but also modify its physical meaning, thus making uncertainty independent of instrumental or experimental contexts (**Ozawa***,* 2003; **Ballentine,** 2014). Some experiments have been performed to verify the accuracy of such new interpretations, thus indicating that the notion above seems to be naive and non-entirely correct (**Erhart *et al,*** 2012; **Rozema *et al*,** 2012). This has inspired an interesting debate about the meaning of the notion of uncertainty (**Bush *et al*,** 2013; **Rozema *et al*,** 2013).

From a different perspective, a new ontology has been recently proposed for single particle interference in ordinary space (**Castañeda & Hurtado,** 2023; **Castañeda *et al*,** 2023; **Castañeda *et al*,** 2021). In this theory, the fundamental role is played by ordinary space, which is conceived as a system with geometric states that confine light and single particles. Such states of space are realized as spatially structured Lorentzian wells, resulting from vacuum fluctuations. The wells become filled of light or particles after a significant number of individual experimental realizations, that is the segments of an interference experiment that begin with the local emission of a single photon or matter particle and end with its local detection, so that only one particle moves in the interferometer without connection with preceding or posterior particles (***Castañeda et al,*** 2023). So, recording of light or particles by a squared modulus detector, placed at a given well cross-section, reveals the structure of the geometric state of space, called interference pattern. In this context, diffraction is shown as a particular case of interference. The main goal of this paper is to discuss new meanings of uncertainty in the framework of this novel ontology.

Fundamentals

Mathematical formalism used in the following is deduced in detail in (**Castañeda *et al,*** 2023) and therefore, its deduction is not included here but its main expressions are directly applied. Let us consider interference in the volume delimited by the mask plane M and the detector plane D, separated a distance z to each other, **figure 1**.

It has been shown that non-locality at M is the necessary and sufficient condition for producing interference in MD volume (**Castañeda *et al,*** 2021). It is represented by functions denoted as $\kappa(\xi_+,\xi_-) = w(\xi_+,\xi_-)\,\tau(\xi_+,\xi_-)$, that link pairs of points of M, specified as $\xi_\pm = \xi_A \pm \xi_D$ 2 in reduced coordinates, i.e. ξ_D denotes the separation vector of the pair of points and ξ_A is the midpoint between them. $w\ \xi_+,\xi_-\ =\ \xi_+\ \psi\ \ \psi\ \xi_-$ is the prepared non-locality at M, with $\langle\xi|\psi\rangle$ the eigenfunction of Laplacian in Helmholtz equation $\nabla^2\langle\xi|\psi\rangle = -k^2\langle\xi|\psi\rangle$, with eigenvalue $-k^2$ and $k = \omega/c$ for light waves of frequency ω (c is the light speed in vacuum) and $k = p/\hbar$ for single matter particles of momentum p (Helmholtz equation is the spatial component of both the wave equation and Schrödinger equation (**Born & Wolf,** 1993; **Feynman *et al.,*** 1965)). The area of pairs of points with the same midpoint ξ_A, for which $w(\xi_+,\xi_-)$ takes on non-negligible values, is called non-locality support. Outside it, $w(\xi_+,\xi_-)$ nullifies or takes on negligible values. $\tau(\xi_+,\xi_-) = t(\xi_+)\,t^*(\xi_-)$ is the non-local transmission function of the mask placed at M. It should be noted that $\kappa(\xi_+,\xi_-) = \kappa^*(\xi_-,\xi_+)$. Local component of non-locality function, obtained by evaluating it for $\xi_D = 0$, gives $\kappa(\xi_A,\xi_A) = w(\xi_A,\xi_A)\,\tau(\xi_A,\xi_A)$ with $w(\xi_A,\xi_A) = |\psi(\xi_A)|^2$, $\tau(\xi_A,\xi_A) = |t(\xi_A)|^2$, and $0 \leq |t(\xi_A)|^2 \leq 1$ the mask transmittance (**Born & Wolf,** 1993) at ξ_A.

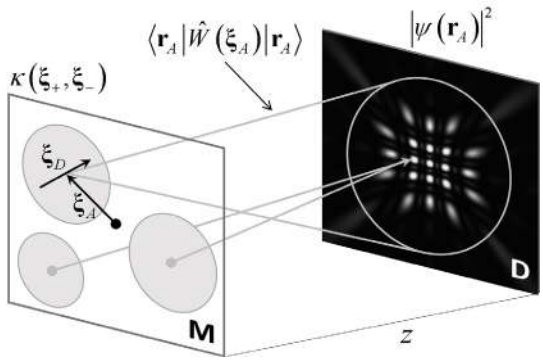

Figure 1. Conceptual sketch for interference in the volume delimited by M and D. Shadowed circles on M represent the non-locality supports. The cone with vertex at ξ_A represents the spatially structured Lorentzian well of the individual geometric state of space that confine light energy or single particles that enter at ξ_A. Mathematical expressions are explained in text.

Interference patterns are locally measured by squared modulus detectors at each point $\mathbf{r}_A$ of D. They are represented by the observable (**Castañeda *et al*,** 2023)

$\mathbf{r}_A$

$$|\psi(\mathbf{r}_A)|^2 = \langle \mathbf{r}_A|\psi\rangle\langle\psi|\mathbf{r}_A\rangle = \int_M d^2\xi_A \langle \mathbf{r}_A|\hat{W}(\xi_A)|\mathbf{r}_A\rangle = \int_M d^2\xi_A \left(\langle \mathbf{r}_A|\hat{R}(\xi_A)|\mathbf{r}_A\rangle + \frac{1}{2}\langle \mathbf{r}_A|\hat{G}(\xi_A)|\mathbf{r}_A\rangle \right). \quad (1)$$

Density operator

$$\hat{W}(\xi_A) = \hat{W}^\dagger(\xi_A) = \hat{R}(\xi_A) + \frac{1}{2}\hat{G}(\xi_A), \quad (2)$$

with † denoting adjoint, represents the individual excited states of space, resulting by exciting each base state of space by specific modes of the geometric potential. Indeed,

$$\hat{R}(\xi_A) = \hat{R}^\dagger(\xi_A) = |\psi(\xi_A)|^2 |t(\xi_A)|^2 \left|\Theta(\xi_A)\right\rangle\left\langle\Theta(\xi_A)\right| \quad (3)$$

and

$$\hat{G}(\xi_A) = \hat{G}^\dagger(\xi_A) = \int_{\substack{M \\ \xi_D \neq 0}} d^2\xi_D \, \kappa(\xi_+,\xi_-) \left|\Theta(\xi_+)\right\rangle\left\langle\Theta(\xi_-)\right|. \quad (4)$$

are the density operators for base states of space and geometric potential, respectively. The projection of self-adjoint kernel $\left|\Theta(\xi_+)\right\rangle\left\langle\Theta(\xi_-)\right|$ on detection points of D gives the scalar, geometric and deterministic function

$$\langle \mathbf{r}_A|\Theta(\xi_+)\rangle\langle\Theta(\xi_-)|\mathbf{r}_A\rangle = \left(\frac{k}{4\pi}\right)^2 \left(\frac{z+|\mathbf{z}+\mathbf{r}_A-\xi_+|}{|\mathbf{z}+\mathbf{r}_A-\xi_+|^2}\right)\left(\frac{z+|\mathbf{z}+\mathbf{r}_A-\xi_-|}{|\mathbf{z}+\mathbf{r}_A-\xi_-|^2}\right)\exp\left(ik|\mathbf{z}+\mathbf{r}_A-\xi_+|-ik|\mathbf{z}+\mathbf{r}_A-\xi_-|\right), \quad (5)$$

whose local component, obtained by evaluating it for $\xi_D = 0$, gives

$$\langle \mathbf{r}_A|\Theta(\xi_A)\rangle\langle\Theta(\xi_A)|\mathbf{r}_A\rangle = \left(\frac{k}{4\pi}\right)^2 \left(\frac{z+|\mathbf{z}+\mathbf{r}_A-\xi_A|}{|\mathbf{z}+\mathbf{r}_A-\xi_A|^2}\right)^2. \quad (6)$$

Equation (6) describes the Lorentzian well with vertex at ξ_A, that realizes the individual base state of space $\langle \mathbf{r}_A|\hat{R}(\xi_A)|\mathbf{r}_A\rangle$ in MD volume, which confines light energy or single particles that enter it at its vertex, represented by coefficient $|\psi(\xi_A)|^2|t(\xi_A)|^2$ in Eq. (3). Equation (5) describes the mode of geometric potential $\langle \mathbf{r}_A|\hat{G}(\xi_A)|\mathbf{r}_A\rangle$ in MD volume, related to the pair of points $\xi_\pm$, in such a way that, if $\kappa(\xi_+,\xi_-)\neq 0$ then the geometric potential mode equally excites (spatially modulates) the base states with vertices at both points $\xi_\pm$. Therefore, $\hat{R}(\xi_A)$ and $\hat{G}(\xi_A)$ are independent to each other, so that $\left[\hat{R}(\xi_A),\hat{G}(\xi_A)\right]=0$, and $\hat{W}(\xi_A)=\hat{R}(\xi_A)$ if $\kappa(\xi_+,\xi_-)=0$ for any $\xi_D \neq 0$.

By expressing $\kappa(\xi_+,\xi_-) = |\kappa(\xi_+,\xi_-)|\exp(i\alpha(\xi_+,\xi_-))$ and considering the Hermitic symmetry of Eq. (4) for the permutation $\xi_\pm \to \xi_\mp$ of any pair of points, i.e. for the two degrees of freedom in orientation of separation vectors, Eq. (4) can be expressed as

Revista de la Academia Colombiana de Ciencias Exactas, Físicas y Naturales.
47(185):795-806, octubre-diciembre de 2023. doi: https://doi.org/10.18257/raccefyn.1952

$$\left\langle \mathbf{r}_A \middle| \hat{G}\left(\xi_A\right) \middle| \mathbf{r}_A \right\rangle = 2 \int\limits_{\substack{M \\ \xi_D \neq 0}} d^{\,2}\xi_D \left|\kappa\left(\xi_+,\xi_-\right)\right| \mathrm{Re}\left(\left\langle \mathbf{r}_A \middle| \Theta\left(\xi_+\right)\right\rangle \left\langle \Theta\left(\xi_-\right) \middle| \mathbf{r}_A \right\rangle \exp\left(i\alpha\left(\xi_+,\xi_-\right)\right)\right), \quad (7)$$

by adding the contributions for the two degrees of freedom in orientation of separation vectors. Re denotes the real part. Integrand of Eq. (7) means that each geometric potential mode excites the base states of space with vertices at a given pair of points $\xi_{\pm}$ with the same cosine-like spatial modulation. However, the spatial structures of the excited states are mirror symmetrical to each other due to the positions of their vertices, as shown later.

Because of geometric potential $\left\langle \mathbf{r}_A \middle| \hat{G}\left(\xi_A\right) \middle| \mathbf{r}_A \right\rangle$, the individual excited states are realized as spatially structured Lorentzian wells $\left\langle \mathbf{r}_A \middle| \hat{W}\left(\xi_A\right) \middle| \mathbf{r}_A \right\rangle$, i.e. the excitation distributes the confinement in specific zones within the base state volume. As a consequence, light energy and single particle quantum probability concentrate in such specific confinement zones.

Excitation uncertainty

Let us consider Young interference with two pinhole mask, with separation vector $\xi_D = \mathbf{a}$, whose non-local transmission function is $\tau\left(\xi_+,\xi_-\right) = \left(\delta\left(\xi_A - \mathbf{a}/2\right) + \delta\left(\xi_A + \mathbf{a}/2\right)\right)\delta\left(\xi_D\right) + \left(\delta\left(\xi_D - \mathbf{a}\right) + \delta\left(\xi_D + \mathbf{a}\right)\right)\delta\left(\xi_A\right)$, with $\delta(\bullet)$ the Dirac delta. First two terms with factor $\delta\left(\xi_D\right)$ are the local component (i.e. transmission function of individual pinholes), while remaining terms with factor $\delta\left(\xi_A\right)$ are the non-local component with the two degrees of freedom in orientation for the separation vector. By inserting this non-local transmission in integrand of Eq. (1), the spatially structured wells of the two individual excited states of space in Young interference become

$$\begin{aligned}\left\langle \mathbf{r}_A \middle| \hat{W}\left(\xi_A\right) \middle| \mathbf{r}_A \right\rangle = {} & \left(\frac{k}{4\pi}\right)^2 \left|\psi\left(\xi_A\right)\right|^2 \left(\frac{z + \left|\mathbf{z} + \mathbf{r}_A - \xi_A\right|}{\left|\mathbf{z} + \mathbf{r}_A - \xi_A\right|^2}\right)^2 \delta\left(\xi_A \pm \mathbf{a}/2\right) \\ & + \left(\frac{k}{4\pi}\right)^2 \left|\kappa\left(\xi_A + \mathbf{a}/2\,,\, \xi_A - \mathbf{a}/2\right)\right| \left(\frac{z + \left|\mathbf{z} + \mathbf{r}_A - \left(\xi_A + \mathbf{a}/2\right)\right|}{\left|\mathbf{z} + \mathbf{r}_A - \left(\xi_A + \mathbf{a}/2\right)\right|^2}\right) \left(\frac{z + \left|\mathbf{z} + \mathbf{r}_A - \left(\xi_A - \mathbf{a}/2\right)\right|}{\left|\mathbf{z} + \mathbf{r}_A - \left(\xi_A - \mathbf{a}/2\right)\right|^2}\right) \\ & \times \cos\left(k\left|\mathbf{z} + \mathbf{r}_A - \left(\xi_A + \mathbf{a}/2\right)\right| - k\left|\mathbf{z} + \mathbf{r}_A - \left(\xi_A - \mathbf{a}/2\right)\right| + \alpha\left(\xi_A + \mathbf{a}/2\,,\, \xi_A - \mathbf{a}/2\right)\right) \delta\left(\xi_A\right)\end{aligned} \quad (8)$$

First term of Eq. (8) describes the Lorentzian wells with vertices at $\xi_A = \pm\mathbf{a}/2$ of base states of space, while the second term points out that Young interference is monomodal and, the geometric potential mode with vertex at the midpoint between pinholes, $\xi_A = 0$, equally excites the two base states.

Cross-section of the overlapped excited states of space at D determines the observable defined Eq. (1) for the Young interference pattern,

$$\left|\psi\left(\mathbf{r}_A\right)\right|^2 = \left\langle \mathbf{r}_A \middle| \hat{W}\left(\frac{\mathbf{a}}{2}\right) \middle| \mathbf{r}_A \right\rangle + \left\langle \mathbf{r}_A \middle| \hat{W}\left(-\frac{\mathbf{a}}{2}\right) \middle| \mathbf{r}_A \right\rangle = \left\langle \mathbf{r}_A \middle| \hat{R}\left(\frac{\mathbf{a}}{2}\right) \middle| \mathbf{r}_A \right\rangle + \left\langle \mathbf{r}_A \middle| \hat{R}\left(-\frac{\mathbf{a}}{2}\right) \middle| \mathbf{r}_A \right\rangle + \left\langle \mathbf{r}_A \middle| \hat{G}(0) \middle| \mathbf{r}_A \right\rangle. \quad (9)$$

A very important feature of Young interference is the dependence of geometric potential from pinhole separation. Specifically, there is an inverse relationship between the excitation spatial frequency and the pinhole separation. Because Lorentzian envelope restricts the angular spreading of excitation modulation, it should be expected that the geometric potential mode does not provide spatial modulation for pinhole separation $|\mathbf{a}| \leq a_0$, with a_0 to be specified. More precisely, for $|\mathbf{a}| \leq a_0$ it takes on only positive values within Lorentzian envelope, instead of varying between positive and negative values. It is illustrated in **figure 2**.

Cosine-like characteristic interference excitation, provided by geometric potential mode for $|\mathbf{a}| > \lambda$ (**Castañeda,** 2017), is shown in (a). After shortening pinhole separation to $|\mathbf{a}| > \lambda$ in (b), only a wider axial main confinement zone is excited together with some lateral zones of low confinement. This geometric potential provides the characteristic diffraction excitation (**Castañeda,** 2017). By further shortening pinhole separation, spatial modulation of geometric potential become significantly smooth and axial main confinement zone

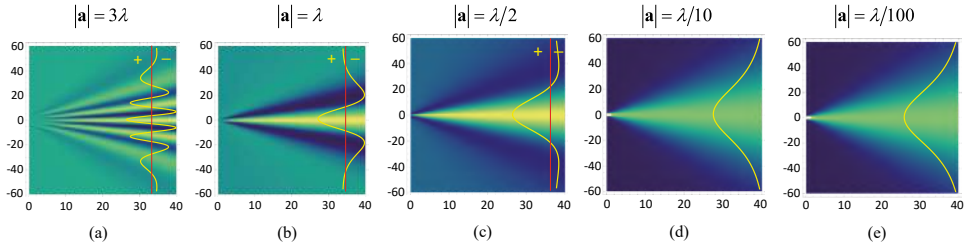

Figure 2. Axial sections of geometric potential for Young interference with different pinhole separation $|\mathbf{a}|$ (λ= 4μm for light waves and photons, and λ= 4pm for single matter particles). Vertical profiles show the spatial modulation excited at $z = 10\lambda$. Horizontal axis $0 \leq z \leq 10\lambda$. Vertical axes are the components of ξ_A on left side and r_A on right side mutually parallel to the pinhole separation vector. Axes units are μm for light waves and photons, and pm for single matter particles.

increases its angular spreading, as shown in (c). For $|\mathbf{a}| = \lambda/10$ in (d), geometric potential mode takes on only positive values of its Lorentzian envelope, and this behavior remains unchanged for $|\mathbf{a}| < \lambda/10$, graph (e). Therefore, Lorentzian cone of invariant geometry for $|\mathbf{a}| \leq \lambda/10$ seems to be the extreme shape of geometric potential mode.

Figure 3 illustrates the wells of individual states of space in Young interference, excited by geometric potential modes in **figure 2** under maximal prepared non-locality al M. As expected, corresponding graphs in upper and bottom rows are mirror symmetrical to each other, with respect to the well axis, and graphs on columns 1 and 2 from left exhibit negative valued forbidden zones (**Castañeda *et al.*,** 2023). Graphs (a), (f) show that geometric potential for interference excites a set of confinement zones for the propagation of light energy and single particles that enter each individual excited state of space at its vertex. In contrast, diffraction confinement in (b) and (g) occupies only the wider axial main zone, surrounding by zones with lower confinement. In graphs (c), (h), these lateral confinement zones disappear in each individual state of space, and their main axial confinement zones remain narrower than Lorentzian well of corresponding base state. However, for $|\mathbf{a}| \leq \lambda/10$ each individual excited state becomes identical to the base state of space, which indicates that geometric potential is unable to spatially modulate them.

It is confirmed by the complete excited state of space resulting by overlapping the two individual excited states, as illustrated in **figure 4** for the examples in **figure 3**. A set of narrow disjoint confinement zones modulate the Lorentzian well as excited by geometric potential for interference, graph (a). Because of spatial entanglement of individual excited states of space (**Castañeda *et al.*,** 2023), their forbidden zones are reduced to null points between consecutive confinement zones in the complete excited state. So, confinement zones behave as propagation channels for light energy and single particles. A wider main axial zone surrounding by lateral zones with lower confinement modulates the well as excited by the geometric potential for diffraction, graph (b). This confirms diffraction as particular case of interference. Because of geometric potential for $|\mathbf{a}| = \lambda/2$, lateral low confinement zones are removed and axial main zone remains narrower than the base space of state, graph (c). However, for $|\mathbf{a}| = \lambda/10$ graph (d), the complete excited state of space for interference becomes identical to the base state of space with vertex at the midpoint between the pinholes. This remains unchanged for $|\mathbf{a}| < \lambda/10$, graph (e). Therefore, it is completely uncertain if both individual and complete states of space are excited by the geometric potential mode for $|\mathbf{a}| \leq \lambda/10$. This suggests $a_0 = \lambda/10$.

The same behavior occurs by weak prepared non-locality, with the only difference that forbidden zones of both individual excited states are removed. Consequently, confinement zones of the complete excited state of space are not disjoint. Nevertheless, $|\mathbf{a}| \leq \lambda/10$ remains valid as criterion for excitation uncertainty.

Revista de la Academia Colombiana de Ciencias Exactas, Físicas y Naturales.
47(185):795-806, octubre-diciembre de 2023. doi: https://doi.org/10.18257/raccefyn.1952

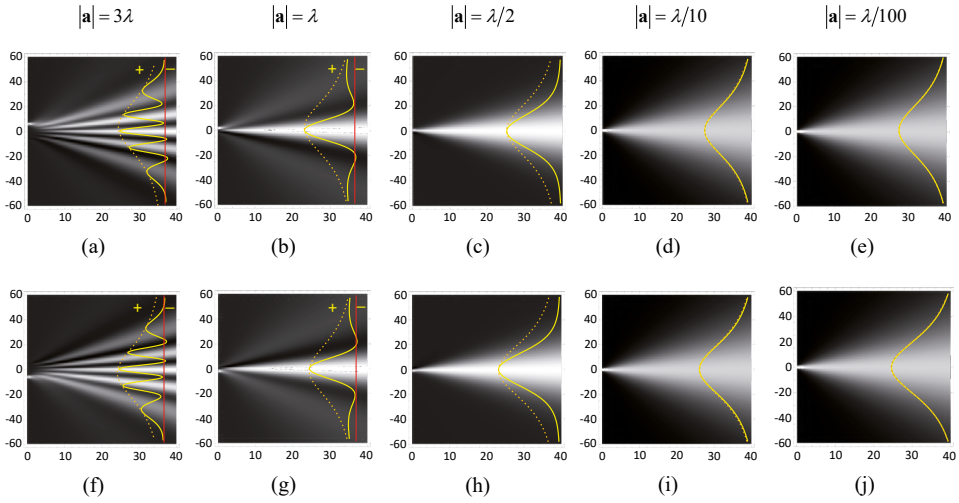

Figure 3. Axial sections of wells of individual states of space in Young interference, excited by geometric potential modes in **figure 2** under maximal prepared non-locality at M. Vertical profiles show well cross-sections at $z = 10\lambda$, which exhibit forbidden zones for $|\mathbf{a}| \geq \lambda$, removed for $|\mathbf{a}| < \lambda$. Dotted line profile describes Lorentzian cross-section of corresponding base state of space. It points out that each individual excited state becomes identical to its base state of space for $|\mathbf{a}| \leq \lambda/10$. Graph axes and units are the same as in **figure 2**.

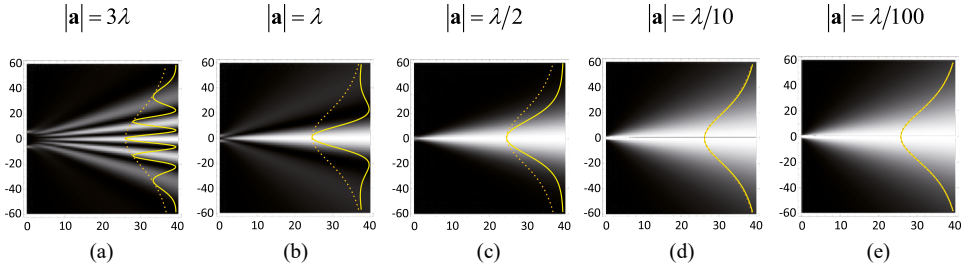

Figure 4. Axial sections of spatially structured Lorentzian wells for Young interference, resulting from overlapping the individual states of space in **figure 3**. It should be noted that spatial structure of each well is identically shaped as the corresponding geometric potential mode in **figure 2**. Vertical profiles show the well cross-sections at $z = 10\lambda$. Dotted line profile describes Lorentzian cross-section of base state of space with vertex at the midpoint between pinholes. Complete excited state of space becomes identical to the base state for $|\mathbf{a}| \leq \lambda/10$. Graph axes and units are the same as in **figure 2**.

The analysis above can be extended for interference with masks with arbitrary distributions of space state vertices. Indeed, each geometric potential mode, activated by arbitrary prepared non-locality, excites only two specific base states of the distribution. As a consequence, Eq. (1) can be expressed as the overlapping of a set of Young interference contributions. It is illustrated without loss of generality in **figure 5**, by considering a mask with a regular 3x3 pinhole array, whose size is determined by the length of array diagonal L. It should be noted that the spatially structured Lorentzian well of the complete excited state of space is shaped by the corresponding geometric potential. For first column on the left, array size and spacing fulfil interference condition $L > |\mathbf{a}| > \lambda$ (**Castañeda,** 2017), so that the spatial modulation of the well cross-sections at any distance z determines an interference pattern after a significant number of individual experimental realizations. For second column from left, diffraction condition $L > \lambda$ and $|\mathbf{a}| < \lambda$ is fulfilled (**Castañeda,** 2017).

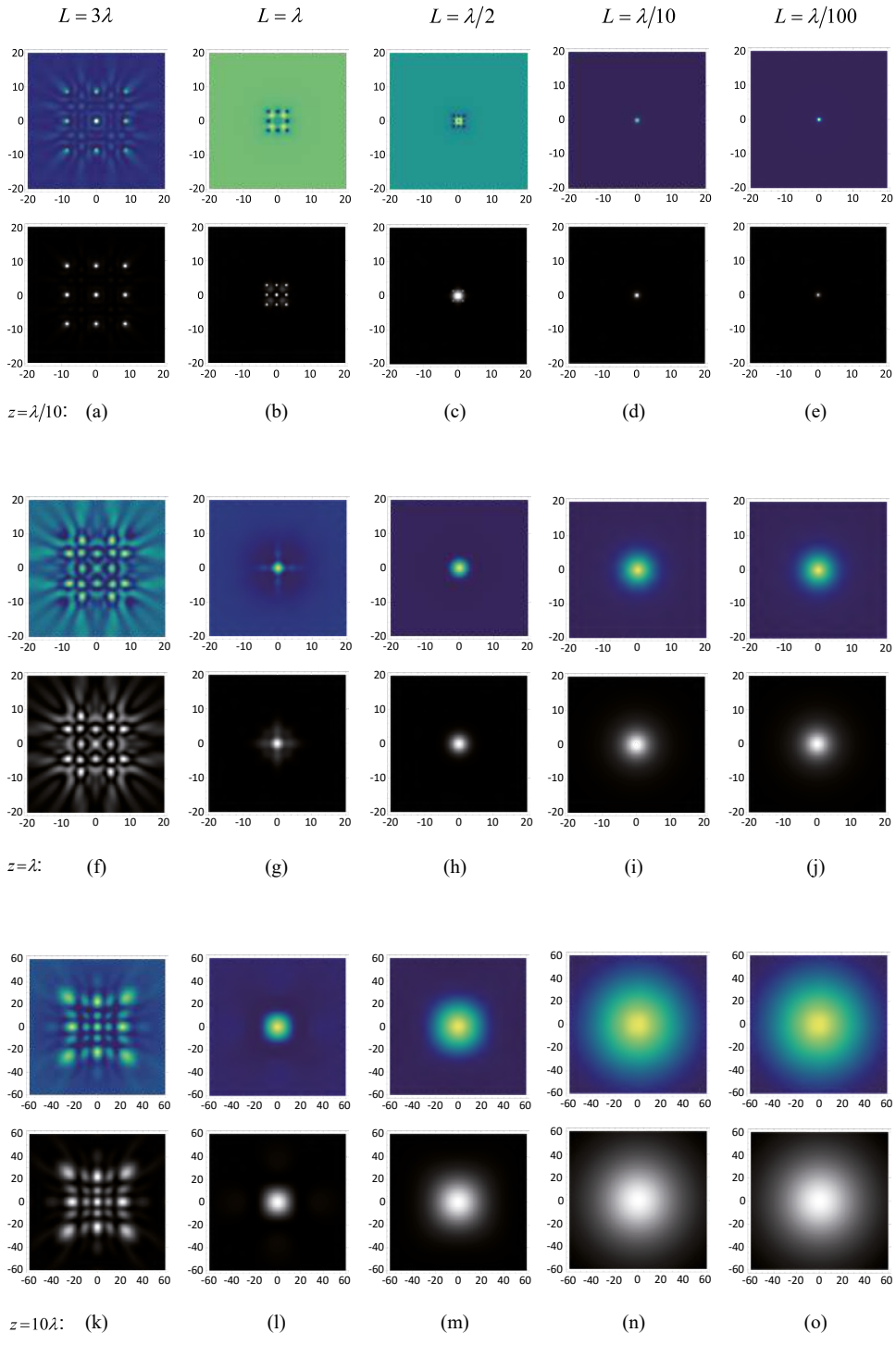

Figure 5. Cross-sections at different distances z of geometric potentials (rows 1, 3, 5 from top) and spatially structured Lorentzian wells (rows 2, 4, 6 from top) for interference with a regular array of 3x3 pinholes under maximal prepared non-locality. Array vertical and horizontal spacing is $|\mathbf{a}| = L/2\sqrt{2}$ (L is the length of array diagonal and λ = 4μm for light and single photons and 4pm for single matter particles). Horizontal and vertical axes are the cartesian components of $\mathbf{r}_A$. Axes units are μm for light waves and single photons, and pm for single matter particles.

Revista de la Academia Colombiana de Ciencias Exactas, Físicas y Naturales.
47(185):795-806, octubre-diciembre de 2023. doi: https://doi.org/10.18257/raccefyn.1952

Well cross-sections at $z \geq \lambda$ in (g), (l) exhibit the characteristic shape of diffraction patterns, that is main axial confinement zone surrounding by zones of lower confinement. However, an important feature is appreciated at very short distance from the mask, graphs (b), i.e. array discreteness. This confirms the notion that discreteness of individual space states is required for diffraction (**Castañeda,** 2017). Indeed, for $|\mathbf{a}| < L < \lambda$, graphs on third column from left, geometric potential provides a smooth modulation for the excited sate of space, i.e. the lateral zones disappear and the main axial confinement zone becomes wider, although array discreteness remains appreciable at very short distance from mask.

For $L \leq \lambda/10$, graphs in columns 4 and 5 from left, array discreteness is not appreciable even at $z = \lambda/10$ and complete excited state of space becomes identical to the base state of space with vertex at any of the nine pinholes, no matter that the pinhole array is under maximum prepared non-locality. The invariance of this behavior for array sizes $L \leq \lambda/10$ allows us generalizing the geometrical excitation uncertainty by this inequality. Specifically, it is completely uncertain that any set of individual states of space with vertices distributed on an area of size $L \leq \lambda/10$ is excited by a geometric potential, because the geometric state of space resulting from their overlapping is identical to the base state of space with vertex at any point in the distribution area. It is useful to assume the vertex position of complete space state at the array midpoint, even if this point is not the vertex of an individual geometric state of set.

The independence of this result from physical and statistical properties of light, single photons and single matter particles propagating in the interferometer leads to the following discussion, related to the use of diffraction as proof of Heisenberg's uncertainty principle (**Feynman *et al.*,** 1965; **Matteucci *et al.*,** 2010). **Figures 4 and 5** show that angular spreading of the main axial confinement zone increases as the size of vertex array of individual excited states of space diminishes. By single matter particle interference, vertex array is considered a set of points for eventual particle crossings through the mask at M. So, in quantum mechanics context, vertex array size can be connected with particle position uncertainty at M. Furthermore, the angular spreading of far-field diffraction central maximum is connected with the uncertainty of the transversal component of the particle momentum. Thus, the inverse relationship between the array size and the central maximum angular spreading has been interpreted as a proof of Heisenberg's uncertainty principle, which formalizes a fundamental quantum attribute of particles. It is reasonable to propose such connections because, in each individual experimental realization, particle should enter only one of the individual states of space at its vertex, and propagates through the space state confined in any of its zones. So, by considering the particle arrival to the mask as a statistical event, the vertex array at M should constitute an area of particle position uncertainty, that could be interpreted as the position uncertainty for the particle at the mask. Furthermore, particle is free of propagating along any path, under the condition that the path remains contained within the main axial confinement zone of the excited state for diffraction. Paths can be distinguished by their transversal components, determined by momentum transversal component. Nevertheless, the specific path following by the particle on propagation is unknown, which means that transversal momentum component is uncertain.

Despite this compatibility between Heisenberg's principle and space states for diffraction, there are significant differences between them. It has been proved that the vertex array is specified by the setup configuration, the geometric potential is activated by the prepared non-locality at the mask and diffraction is determined by the vertex array size and spacing, independently of physical and statistical attributes of particles. All these features are formalized by deterministic parameters, that specify the spatial structure of the excited state of space, which in turn results in the setup as a consequence of vacuum fluctuations (**Castañeda & Hurtado,** 2023). In addition, the limit $L \leq \lambda/10$ of the set of excited states of space has been not considered in quantum mechanics, because its paraxial approach is unable to account for it. This limit seems to restrict the use of diffraction in connection with Heisenberg's principle, because for $L \leq \lambda/10$ the angular spreading of the well is maximal and remains fixed (~68.5° for a decay in ~95% (**Castañeda,** 2017)), and the well cross-section remains Lorentzian.

Vertex position uncertainty

In absence of prepared non-locality, geometric potential is not activated so that $\langle \mathbf{r}_A | \hat{G}(\xi_A) | \mathbf{r}_A \rangle = 0$ and Eq. (1) reduces to the overlapping of base states of space, i.e.

$$|\psi(\mathbf{r}_A)|^2 = \int_M d^2\xi_A \langle \mathbf{r}_A | \hat{R}(\xi_A) | \mathbf{r}_A \rangle = \left(\frac{k}{4\pi}\right)^2 \int_M d^2\xi_A |\psi(\xi_A)|^2 |t(\xi_A)|^2 \left(\frac{z + |\mathbf{z} + \mathbf{r}_A - \xi_A|}{|\mathbf{z} + \mathbf{r}_A - \xi_A|^2}\right)^2 . \quad (10)$$

Equation (10) points out that base states of space cannot induce spatially modulations on them. Moreover, at long enough distance from M, the cross-section geometry of overlapped base states equals the geometry of the cross-section of an individual base state, independently of the number of overlapped base states and the distribution of their vertices at M. It is illustrated in **figure 6** for two base states and generalized in **figure 8** by considering an array of 3x3 base states. So, the connection between diffraction and Heisenberg's principle seems to be feasible by providing $\kappa(\xi_+, \xi_-) \neq 0$, $L > \lambda$ and $|\mathbf{a}| < \lambda$. For $\kappa(\xi_+, \xi_-) = 0$, the angular spreading of far-field diffraction is maximal, i.e. identical to the Lorentzian well of a base space. Indeed, **figure 6** shows the excellent fit, at $z = 10\lambda$, between the cross-section profile of the overlapped base states of space and the individual base state with vertex at the midpoint between the mask pinholes.

Figures 6, 7 show a further feature of geometric uncertainty, involved in Eq. (10). **figure 6** points out that, for each pinhole separation, there is a finite distance z_0 so that the two base states can be distinguished for $z \leq z_0$. In addition, $z_0 \to 0$ as $|\mathbf{a}| \to 0$. Therefore, it should be interesting to analyze the distinguishability related to the excitation uncertainty $|\mathbf{a}| < \lambda/10$.

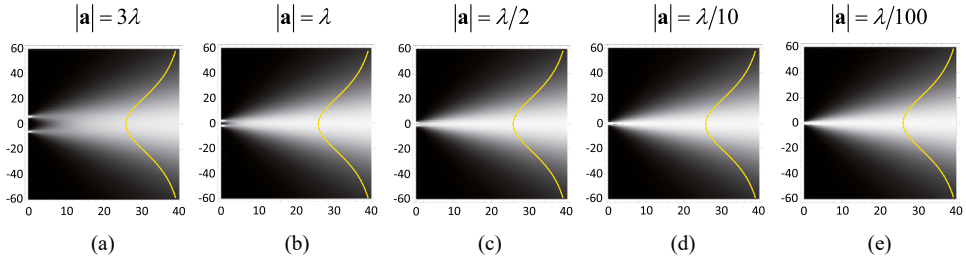

Figure 6. Axial sections of the overlapping of base states of space in Young interference, for different pinhole separations $|\mathbf{a}|$. Vertical profiles compare, at $z = 10\lambda$, the cross-sections of the overlapped wells (solid line) with the Lorentzian cross-section of the base state of space with vertex at the midpoint between the mask pinholes (dotted line). The overlapped state of space becomes identical to the base state for $|\mathbf{a}| \leq \lambda/10$. Graph axes and units are the same as in **figure 2**.

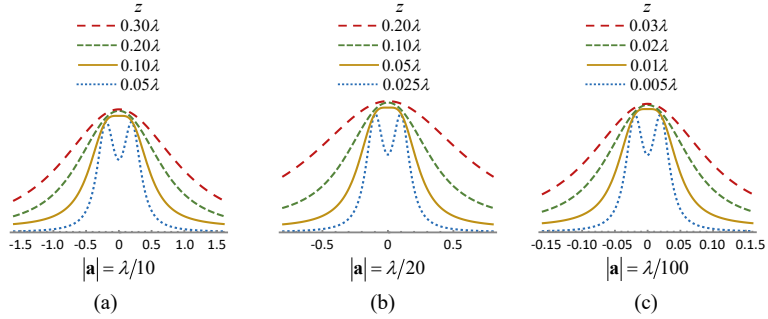

Figure 7. Cross-section profiles at different distances z, of the overlapping of base states in Young interference, for different pinhole separations $|\mathbf{a}| \leq \lambda/10$. In all cases, solid line profile with flat maximum is corresponding to $z = |\mathbf{a}|$. For $z < |\mathbf{a}|$ the profiles exhibit two distinguishable maxima, corresponding to each base state. For $z > |\mathbf{a}|$ the profiles become Lorentzian, so that the two base states are not distinguishable.

Revista de la Academia Colombiana de Ciencias Exactas, Físicas y Naturales.
47(185):795-806, octubre-diciembre de 2023. doi: https://doi.org/10.18257/raccefyn.1952

Cross-section profiles in **figure 7** describe the overlapping of two base states of space along a very short distance from mask, $z \leq 0.3\ \lambda$, for pinhole separations $|\mathbf{a}| \leq \lambda/10$. They suggest to consider $z = |\mathbf{a}|$ as limit distance for base state distinguishability. Profile at this limit distance exhibits a flat maximum, which evolve to two maxima along $z < |\mathbf{a}|$ corresponding to distinguishable base states, and to only one acute maximum along $z > |\mathbf{a}|$, so that the two base states become undistinguishable to each other, and the overlapped state exhibits the same geometry as the individual base state with vertex at the midpoint between the pinholes.

This geometrical non-distinguishability can be interpreted as base state vertex position uncertainty, because the Lorentzian wells of all the base states with vertices in the area of radius $r = \lambda/10$ centered at a given point are identical to the Lorentzian well of the individual base estate with vertex at the center for $z \geq \lambda/10$. In other words, the Lorentzian well remains invariant no matter the position of its vertex in such area, and therefore, its vertex position is completely uncertain within such area. As a consequence, single particles that arrive to any point within the uncertainty area become confined in the base state with vertex at the area center, no matter the statistics of the particle arrivals.

The analysis above can be generalized to any set of base states of space, with an arbitrary distribution of vertices of size L in the mask. So, if $L \leq \lambda/10$ then all the base states of space are represented by the individual Lorentzian well with vertex at the midpoint of the array. It is illustrated in **figure 8** for an array of 3x3 vertices at M. Graph (d) is the cross-

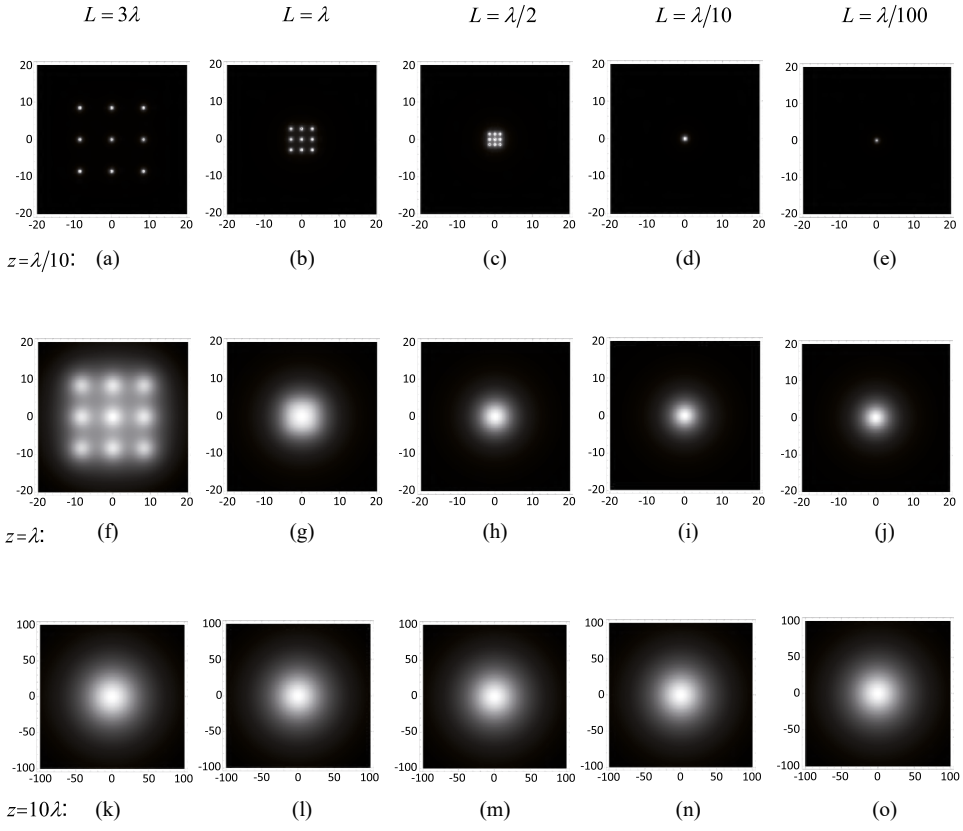

Figure 8. Cross-sections at different distances z of the overlapping of Lorentzian wells with vertices at the 3x3 pinhole array of a mask placed at M. Array vertical and horizontal spacing is $|\mathbf{a}| = L/2\sqrt{2}$ (L is the length of the array diagonal and $\lambda = 4\mu m$ for light and single photons and 4pm for single matter particles). Horizontal and vertical axes are the cartesian components of $\mathbf{r}_A$. Axes units are μm for light waves and single photons, and pm for single matter particles.

section at the distinguishability limit $z = L = \lambda/10$, so that the 3x3 array is distinguishable in (a)-(c) and remains undistinguishable in (e). Graphs on bottom row, $z = 10\lambda$, show that cross-sections of all the arrays are identical to the Lorentzian cross-section of the individual base state with vertex at the array midpoint. Graphs on columns for $L \leq \lambda/10$ indicate that Lorentzian well of overlapped state of space remains identical to Lorentzian well of this individual base state along $z \geq \lambda/10$.

It is worth clarifying the difference between vertex position uncertainty and resolution limit. The term resolution limit refers to quantitative descriptors of the ability of an optical system (mainly imaging and spectroscopy systems) to distinguish fine details (**Born & Wolf,** 1993). Therefore, resolution limit is a characteristic of optical system performance. Geometric uncertainty refers to a property of the states of ordinary space, described by the quantitative limit $L \leq \lambda/10$, with L the size of state vertex array. If this condition is satisfied, then the complete array behaves as an individual base state, whose vertex can be placed in any of the array points, even at the center of the array no matter that this point is not the vertex of a space state of the array, and no matter the prepared no-locality on the mask plane. So, both the excitation provided by the geometric potential and the vertex position of the space state are completely uncertain, although the vertices of the array can be resolved for $z < \lambda/10$, as illustrated by profiles in **figure 7**.

An interesting connection between Heisenberg's principle and geometric uncertainty can be appreciated by considering $\Delta x = \lambda/10$, with Δx Heisenberg's position uncertainty. Therefore, Heisenberg's principle leads to $\Delta p \geq \frac{\hbar}{2\Delta x}$, i.e. $\Delta p \geq \frac{5h}{2\pi\lambda}$ and, by using de Broglie's formula $p = h/\lambda$ (**Feynman *et al.,*** 1965), it gives $\Delta p \geq 0.7958\, p$ for Heisenberg's momentum uncertainty. By considering the particle confinement in the base state of space due to the Heisenberg's position uncertainty, and assuming the particle enters the base state with the momentum parallel to the Lorentzian well axis, then Δp should be contained in the angular spreading of the base state. It means $\Delta p = p \sin 68.5° = 0.9304\, p$, which is compatible with Heisenberg's principle. Nevertheless, this result has a further meaning, not implied by Heisenberg's principle, i.e. it seems to establish an upper limit for Δp due to the geometry of the Lorentzian well of base state of space. In addition, the position uncertainty $\Delta x = \lambda/10$ cannot be reduced by using smaller openings because arrays of points with sizes $L \leq \lambda/10$ are associated to a unique base state of space with a fixed Lorentzian geometry. Thus, $\lambda/10$ seems to be the lower limit for Δx. Such extreme limits for the notion of uncertainty due to the geometrical properties of states of space are proposed for the first time in this paper.

Conclusion

The notion of geometric uncertainty has been discussed in the framework of the non-paraxial interference theory based on confinement in geometric states of space. This notion refers to two important features of any set of excited states of space, whose vertices distribute in an arbitrary array of size L, and is formalized by the condition $L \leq \lambda/10$. If this condition is fulfilled, then both the excitation provided by the geometric potential and the vertex position of the states become completely uncertain, i.e. the set of states (i) are not spatially modulated, even under maximal prepared non-locality, and (ii) are represented by the Lorentzian well of an individual base state of space with vertex at any point of the array (it is useful to assume the vertex of this well at the midpoint of the array, even if this point is not a vertex of any state of the set). Geometric uncertainty is different but compatible with Heisenberg's uncertainty principle. In fact, it establishes both the upper limit for Heisenberg's momentum uncertainty and the lower limit for Heisenberg's position uncertainty. It should be mentioned that the limit $\lambda/10$ is a criterion established by numerically comparing the geometries of the base state and the excited states of ordinary space. Descriptors like the rms-value for cross-section comparison at $z \geq \lambda/2$ support this limit with a precision of order 95%.

Conflicts of interest

Author declares no conflicts of interest.

Data availability

No data were generated or analyzed in the presented research.

Funding Statement

This work was carried out under research program Semillero 2241 - Ciencia de la Luz of Universidad Nacional de Colombia.

References

Ballentine L. (2014). Quantum Mechanics: A Modern Development, 2nd ed. World Scientific.

Born, M., Wolf, E. (1993). Principles of Optics 6th ed. Oxford: Pergamon Press.

Busch, P., Lahti, P., Werner, R.F. (2013). Proof of Heisenberg's Error-Disturbance Relation. *Physical Review Letters, 111,* 160405.

Castañeda, R., Hurtado, C. (2023). Vacuum fluctuations in single photon interference. Submitted to Journal Mod. Opt.

Castañeda, R., Bedoya, P., Hurtado, C. (2023). Quantum formalism of interference as confinement in spatially structured Lorentzian wells. Journal of Physics. A: Mathematical and Theoretical, *56*, 045302. https://doi.org/10.1088/1751-8121/acb6c6

Castañeda, R., Bedoya, P., Matteucci, G. (2021). Non-locality and geometric potential provide the phenomenology of the double-hole single massive particle and light interference. *Physica Sripta, 96,* 125036. https://doi.org/10.1088/1402-4896/ac3ea5

Castañeda, R. (2017). Discreteness of the real point emitters as a physical condition for diffraction. *Journal of the Optical Society of America A, 34,* 184-192. https://doi.org/10.1364/JOSAA.34.000184

Erhart, J., Sponar, S., Sulyok, G., Badurek, G., Ozawa, M., Hasegawa, Y. (2012). Experimental Demonstration of a Universally Valid Error-Disturbance Uncertainty Relation in Spin Measurements. *Nature Physics, 8,* 185-189. http://dx.doi.org/10.1038/nphys2194

Feynman, R., Leighton R., Sands, M. (1965). The Feynman Lectures on Physics vol 3. Menlo Park: Addison–Wesley.

Matteucci, G., Ferrari, L., Migliori, A. (2010). The Heisenberg uncertainty principle demonstrated with an electron diffraction experiment. *European Journal of Physics, 31,* 1287-1293. http://iopscience.iop.org/ 0143-0807/31/5/027

Ozawa, M. (2003). Universally valid reformulation of the Heisenberg uncertainty principle on noise and disturbance in measurement. *Physical Review A, 67,* 042105.

Rozema, L.A., Darabi, A., Mahler, D.H., Hayat, A., Soudagar, Y., Steinberg A.M. (2012). Violation of Heisenberg's Measurement-Disturbance Relationship by Weak Measurements. *Physical Review Letters, 109*, 100404.

Rozema, L.A., Mahler, D.H., Hayat, A., Steinberg, A.M. (2013). A Note on Different Definitions of Momentum Disturbance. *arXiv:*1307.3604.